

# Observations of Faint, Hard-Band X-ray Sources in the Field of CRSS J0030.5+2618 with the Chandra X-ray Observatory and the Hobby-Eberly Telescope<sup>1</sup>

W.N. Brandt<sup>2</sup>, A.E. Hornschemeier<sup>2</sup>, D.P. Schneider<sup>2</sup>, G.P. Garmire<sup>2</sup>, G. Chartas<sup>2</sup>, Gary J. Hill<sup>3</sup>, P.J. MacQueen<sup>3</sup>, L.K. Townsley<sup>2</sup>, D.N. Burrows<sup>2</sup>, T.S. Koch<sup>2</sup>, J.A. Nousek<sup>2</sup> and L.W. Ramsey<sup>2</sup>

## ABSTRACT

We present results from a study of 2–8 keV X-ray sources detected by the Advanced CCD Imaging Spectrometer (ACIS) instrument on the *Chandra* X-ray Observatory in the field of the  $z = 0.516$  cluster CRSS J0030.5+2618. In our 63.5 arcmin<sup>2</sup> search area, we detect 10 sources with 2–8 keV fluxes down to  $\approx 4 \times 10^{-15}$  erg cm<sup>-2</sup> s<sup>-1</sup>; our lowest flux sources are  $\approx 10$  times fainter than those previously available for study in this band. Our derived source density is about an order of magnitude larger than previous source counts above 2 keV, although this density may be enhanced somewhat due to the presence of the cluster. We detail our methods for source detection and characterization, and we show that the resulting source list and parameters are robust. We have used the Marcario Low Resolution Spectrograph on the Hobby-Eberly Telescope to obtain optical spectra for several of our sources; combining these spectra with archival data we find that the sources appear to be active galaxies, often with narrow permitted lines, red optical continua or hard X-ray spectra. Four of the X-ray sources are undetected to  $R = 21.7$ ; if they reside in  $L^*$  galaxies they must have  $z > 0.55$ –0.75 and hard X-ray luminosities of  $L_{2-8} \gtrsim 4 \times 10^{42}$  erg s<sup>-1</sup>. We detect all but one of our 2–8 keV sources in the 0.2–2 keV band as well. This result extends to significantly lower fluxes the constraints on any large, completely new population of X-ray sources that appears above 2–3 keV.

*Subject headings:* diffuse radiation — surveys — X-rays: galaxies — X-rays: general

---

<sup>1</sup>Based on observations obtained with the Hobby-Eberly Telescope, which is a joint project of the University of Texas at Austin, the Pennsylvania State University, Stanford University, Ludwig-Maximilians-Universität München, and Georg-August-Universität Göttingen.

<sup>2</sup>Department of Astronomy and Astrophysics, The Pennsylvania State University, University Park, PA 16802

<sup>3</sup>McDonald Observatory, University of Texas, Austin, TX 78712

## 1. Introduction

About 70% of the extragalactic X-ray background in the soft 0.5–2 keV band has been resolved into discrete sources by pencil-beam surveys with the *ROSAT* satellite (e.g., Hasinger et al. 1998). The 0.5–2 keV source counts have reached a surface density of  $\approx 1000 \text{ deg}^{-2}$  at a discrete source detection limit of  $\approx 10^{-15} \text{ erg cm}^{-2} \text{ s}^{-1}$ , and simple extrapolations suggest that all of the 0.5–2 keV extragalactic X-ray background will be resolved by a flux limit of  $\sim 2 \times 10^{-16} \text{ erg cm}^{-2} \text{ s}^{-1}$  at which the surface density will be  $\sim 3000 \text{ deg}^{-2}$ . Optical identification programs (e.g., Schmidt et al. 1998) have established that type 1 Active Galactic Nuclei (AGN), such as Seyfert 1 galaxies and Quasi-Stellar Objects (QSOs), are the dominant contributors above a 0.5–2 keV flux of  $\approx 5 \times 10^{-15} \text{ erg cm}^{-2} \text{ s}^{-1}$ . A non-negligible number (about 16%) of type 2 AGN are seen as well.

Largely due to instrumental limitations, the nature of the sources that produce the  $> 2 \text{ keV}$  X-ray background is much less certain at present. It is important to solve this mystery since most of the energy density in the X-ray background is located above the *ROSAT* band. The best current constraints on the sources of the 2–10 keV X-ray background have come from the *ASCA* and *BeppoSAX* satellites. Long observations with these satellites have resolved discrete source detection limits of  $\approx (3\text{--}5) \times 10^{-14} \text{ erg cm}^{-2} \text{ s}^{-1}$  and have resolved  $\approx 30\%$  of the 2–10 keV background into discrete sources (e.g., Ogasaka et al. 1998; Giommi, Fiore & Perri 1999). The integrated number of sources,  $N$ , is consistent with the law  $N(> S) \propto S^{-3/2}$  expected for a uniform distribution of sources in Euclidean space. The deepest 2–10 keV source counts to date have resolved  $\approx 60$  sources  $\text{deg}^{-2}$ . The faintest 2–10 keV sources appear to have flatter spectra (with energy indices of  $\alpha \approx 0.5 \pm 0.2$ ) than those of typical unabsorbed AGN (e.g., Ueda et al. 1998), suggesting that a population of sources with spectra similar to that of the integrated X-ray background dominates above 2 keV. The population is thought to be at least partially composed of obscured AGN, and some of these hard sources have indeed been associated with such objects (e.g., Fiore et al. 1999; Akiyama et al. 2000). An important result, however, is that the majority of the hard sources found thus far appear to have counterparts in the soft X-ray band (Giommi, Fiore & Perri 1998). Obscured AGN might still create soft X-ray emission via electron-scattered X-rays or due to non-nuclear X-ray emission (e.g. starburst activity).

The arcsecond imaging quality and high-energy sensitivity of the *Chandra* X-ray Observatory (Weisskopf, O’Dell & van Speybroeck 1996) promises to revolutionize our understanding of the X-ray background above 2 keV. The source confusion and misidentification problems that have dogged earlier hard X-ray surveys will be eliminated. In this paper, we use data from *Chandra*, the 8-m class Hobby-Eberly Telescope (HET), and public archives to study a small but well-defined sample of faint X-ray sources in the 2–8 keV band. Our sample contains several of the faintest  $> 2 \text{ keV}$  sources yet detected and identified. We address (1) the number counts at faint hard X-ray fluxes, (2) the nature of the faint hard X-ray sources, and (3) the issue of whether most faint hard X-ray sources have soft X-ray counterparts. Our X-ray sources lie in the PG 0027+260 (an eclipsing cataclysmic variable) field of the Cambridge-Cambridge *ROSAT* Serendipity Survey

(e.g., Boyle, Wilkes & Elvis 1997). This field contains CRSS J0030.5+2618, a  $z = 0.516$  cluster of galaxies, and it was observed by *Chandra* for 44 ks during its first month of calibration-phase operations. The Galactic column density along this line of sight is  $(3.9 \pm 0.4) \times 10^{20} \text{ cm}^{-2}$  (Stark et al. 1992), corresponding to an optical depth of  $\tau < 0.02$  for the 2–8 keV band of primary interest here. In this paper we assume  $H_0 = 70 \text{ km s}^{-1} \text{ Mpc}^{-1}$  and  $q_0 = \frac{1}{2}$ .

## 2. X-ray Observations and Data Analysis

### 2.1. ACIS Observation Details and Image Creation

The field containing CRSS J0030.5+2618 was observed with the *Chandra* Advanced CCD Imaging Spectrometer (ACIS; Garmire & Nousek 1999a; Garmire et al. 2000, in preparation) for a total exposure time of 44 ks on 1999 August 17. ACIS consists of ten CCDs designed for efficient X-ray detection and spectroscopy. Four of the CCDs (ACIS-I; CCDs I0–I3) are arranged in a  $2 \times 2$  array with each CCD tipped slightly to approximate the curved focal surface of the *Chandra* High Resolution Mirror Assembly (HRMA). The remaining six CCDs (ACIS-S; CCDs S0–S5) are set in a linear array and tipped to approximate the Rowland circle of the objective gratings that can be inserted behind the HRMA. The CCD which lies on-axis in ACIS-S (S3) is orthogonal to the HRMA optical axis. It is a back-illuminated CCD that is sensitive for imaging soft X-ray objects. Each CCD subtends an  $8.3' \times 8.3'$  square on the sky. The individual pixels of the CCDs subtend  $\approx 0.5'' \times 0.5''$  on the sky. The on-axis image quality of the telescope is approximately  $0.5''$  (FWHM); this quantity increases to  $\approx 1.0''$  (critical sampling on the detector) at an off-axis angle of  $\approx 2'$ . The image size also has a weak energy dependence, with poorer quality at higher energy.

The observation was performed in two segments (observation ID numbers 1190 and 1226), separated by 1.0 ks. CRSS J0030.5+2618 was placed at the aim point for the ACIS-S array (on CCD S3) during the observation. The aim point position was  $\alpha_{2000} = 00^{\text{h}}30^{\text{m}}32.5^{\text{s}}$ ,  $\delta_{2000} = +26^{\circ}18'13.4''$ . The focal plane temperature was  $-99.3^{\circ}\text{C}$ . Faint mode was used for the event telemetry format, and *ASCA* grade 7 events were rejected on orbit to prevent telemetry saturation (see §5.7 of the *AXAF Observatory Guide* for a discussion of grades). Only one 3.3 s frame was ‘dropped’ from the telemetry.

Here we will focus on the data from CCD S3 since it has not shown the charge transfer inefficiency (CTI) increase that has affected the front-illuminated CCDs (see Garmire & Nousek 1999b). To avoid problems associated with the dither of *Chandra* (see §4.9.2 of the *AXAF Observatory Guide*), we also neglect data within  $20''$  of the edge of S3. Our search area thus comprises 63.5 square arcminutes or 92% of S3. The two observation segments were co-added using the EVENT BROWSER software (Broos et al. 1999). We used the CIAO DATAMODEL software, provided by the *Chandra* X-ray Center, to create  $\approx 0.5'' \text{ pixel}^{-1}$  images in the ‘full’ (0.2–8 keV), ‘soft’ (0.2–2 keV), and ‘hard’ (2–8 keV) bands (neglecting the 8–10 keV data improves the signal-to-noise ratio in the hard band; e.g., Baganoff 1999). Our 0.2, 2, and 8 keV band boundaries

have uncertainties of 80 eV, 20 eV and 160 eV, respectively. These uncertainties are smaller than or comparable to the S3 spectral resolution, and the 0.2 and 8 keV uncertainties are innocuous due to the small effective area of HRMA/ACIS below 0.3 keV and above 8 keV. The 2 keV band boundary is furthermore convenient because it is close to the energy of the HRMA response drop due to the iridium M-edge.

We have only used events with ACIS grades of 0, 2, 8, 16 and 64. For the background level during this observation, this conservative grade set appears to provide the best overall performance when trying to detect faint, hard sources on S3, although we explore other grade set choices in §2.4. For this 44 ks observation, the average background in the hard band varies across S3 in the range  $\approx 0.03\text{--}0.05 \text{ count pixel}^{-1}$ .

We corrected the *Chandra* astrometry by comparison with *ROSAT* HRI, Palomar Optical Sky Survey (POSS), and Isaac Newton Telescope data (see below). The QSO CRSS J0030.6+2620 ( $z = 0.493$ ) and the Seyfert 2 CRSS J0030.7+2616 ( $z = 0.247$ ) were particularly useful in this regard (see Boyle et al. 1995 and Boyle et al. 1997).

## 2.2. Source Searching

We used the CIAO WAVDETECT software (Dobrzański et al. 1999; Freeman et al. 2000) to search our images for sources. Our primary interest is in 2–8 keV point sources. We used a significance threshold of  $1 \times 10^{-6}$  and computed 5 scaled transforms for wavelet scale sizes of 1, 2, 4, 6 and 8 pixels. In our hard band image, we have detected 9 point sources on S3.<sup>4</sup> These are listed in Table 1 and shown in Figures 1 and 2. We estimate that our absolute positions in the hard band are good to within  $\approx 3''$ . They are therefore of comparable quality to those used in the *ROSAT* High-Resolution Imager survey of the Lockman Hole (Hasinger et al. 1998), and they are *much* better than earlier positions in the hard X-ray band. All of these sources, except source 5, were also detected in the independent soft-band image (usually with a significantly higher number of counts), giving us confidence in their reality. The relative positional agreement between hard-band and soft-band sources was typically better than  $1''$ . Given this relative positional agreement, the probability that any given source is a false match is  $\approx 0.2\%$ . While the background in the soft band has significant spatial structure due to instrumental effects (e.g., node boundaries) and the presence of the cluster, this does not appear to affect our matching of hard and soft sources. Source 7 lies at a position where the soft-band background is elevated by  $\approx 25\%$  by the central node boundary. This elevated background arises due to cosmic rays interacting with the physically separated frame store regions of the S3 CCD, and it is blurred when the *Chandra* dither is removed by the pipeline software. The slightly elevated background does not compromise the

---

<sup>4</sup>We also detect a source at  $\alpha_{2000} = 00^{\text{h}}30^{\text{m}}57.8^{\text{s}}$ ,  $\delta_{2000} = +26^{\circ}17'44.3''$ , but this source lies  $\approx 19''$  from the edge of S3 and is hence excluded from consideration.

detection of source 7, but our soft-band photometry may have a small systematic error in addition to the statistical error given in Table 1. In addition, we are confident that none of our sources is due to a ‘hot pixel’ because these would show the characteristic Lissajous dither pattern from the spacecraft aspect. We have compared the angular extents of our sources with the 90% encircled energy radius of the *Chandra* PSF (see §3.8 of the *AXAF Observatory Guide*), and although the photon statistics are limited we find no clear evidence for anomalous extent.

We have compared our number counts in the soft band with those of Hasinger et al. (1998) as a rough consistency check. Hasinger et al. (1998) found  $940 \pm 170$  sources  $\text{deg}^{-2}$  at a 0.5–2 keV flux level of  $1 \times 10^{-15}$   $\text{erg cm}^{-2} \text{s}^{-1}$ . Our source density in the soft band is  $1500 \pm 300$  sources  $\text{deg}^{-2}$  at a 0.2–2 keV flux level of  $\approx 6 \times 10^{-16}$   $\text{erg cm}^{-2} \text{s}^{-1}$ . For plausible bandpass corrections, our number counts are roughly consistent with a simple extrapolation of the Hasinger et al. (1998)  $\log N$ – $\log S$  relation. We note that there is probably an enhancement in our number counts due to the presence of the cluster CRSS J0030.5+2618 (see §4 for further discussion).

The minimum detectable 2–8 keV flux varies across S3 due to effects such as point spread function (PSF) broadening, vignetting, and spatially dependent CTI. Within  $3.5'$  of the aim point, we estimate our flux limit to be  $(4\text{--}5) \times 10^{-15}$   $\text{erg cm}^{-2} \text{s}^{-1}$  (corresponding to  $\approx 6$  counts), while at larger off-axis angles our flux limit increases fairly quickly (e.g., see Figure 6.5 of the *AXAF Proposers’ Guide*). While this spatially dependent flux limit should be kept in mind, none of our main results below is sensitive to the precise details of our flux limit. Even at the locations on S3 furthest from the aim point, the observation is  $\gtrsim 5$  times deeper than previous hard X-ray surveys.

### 2.3. Source Parameterization

WAVDETECT performs photometry on detected sources, and we have cross checked the WAVDETECT results with manual aperture photometry. We find good agreement between the two techniques for all sources other than source 2, where the WAVDETECT photometry clearly has failed (WAVDETECT finds source 2 but claims it only has 0.9 counts in the hard band). In Table 1 we quote our manual photometry results for source 2 and WAVDETECT photometry results for all other sources. These have not been corrected for vignetting. We also quote the ‘band ratio’ defined as the ratio of hard-band to soft-band counts. The errors for our band ratio values have been computed following the ‘numerical method’ described in §1.7.3 of Lyons (1991); in the Poisson limit this method is more reliable than the standard approximate variance formula (e.g., see §3.3 of Bevington & Robinson 1992). In Figure 3 we compare our band ratios to power-law models with varying amounts of neutral absorption. Several of our sources appear likely to suffer significant internal X-ray absorption. In addition, WAVDETECT reports a significance level for each source, defined as the number of source counts divided by the Gehrels (1986) standard deviation of the number of background counts (see Table 1). For source 2 we have calculated the 2–8 keV significance using our manual photometry. We do not report a 0.2–2 keV significance for source 5 because it is not detected in this band.

We have used EVENT BROWSER to create full-band light curves for our sources. We analyzed these for variability using a Kolmogorov-Smirnov test. Most of our sources do not show significant evidence for variability. Source 8 may show variability by a factor of  $\approx 2$  on a timescale of  $\approx 10000$  s. The fact that the photon arrival times for our sources are distributed fairly evenly throughout the observation length is a further argument against some brief, transient effect (e.g., a transient ‘hot pixel’ or a cosmic ray) producing spurious sources. We have also examined the energy and ACIS grade distributions for our sources and find no anomalies that might indicate spurious instrumental effects.

We have calculated vignetting-corrected 0.2–2 keV and 2–8 keV fluxes for our sources using the counts from Table 1, and these are given in Table 2. We assume a  $\Gamma = 1.9$  power-law model with the Galactic column density, and our fluxes have not been corrected for Galactic or internal absorption. Our 2–8 keV observed fluxes (those of primary scientific interest here) are quite insensitive to the assumed column density for  $N_{\text{H}} \lesssim 10^{22} \text{ cm}^{-2}$  (compare with Figure 3). Our 0.2–2 keV fluxes are somewhat more sensitive to the assumed column density; for our sources with large band ratios the 0.2–2 keV fluxes calculated with Galactic absorption are 5–20% lower than those calculated using  $\Gamma = 1.9$  and column densities estimated from Figure 3. For our flux calculations, we have used the calibration-phase ACIS redistribution matrix files (rmfs) from the ACIS calibration group (S. Buczkowski & N. Schulz, private communication), and we have also used the calibration-phase ancillary response files (arfs; N. Schulz, private communication). These spectral responses are for a focal plane temperature of  $-100^{\circ}\text{C}$ , and they assume filtering upon *ASCA* grades 0, 2, 3, 4 and 6. To correct for our more conservative choice of grades, we have multiplied our 0.2–2 keV fluxes by a factor of  $1.23 \pm 0.12$  and our 2–8 keV fluxes by a factor of  $1.53 \pm 0.23$  (statistical errors only). These factors have been determined by comparing the numbers of events for our sources obtained with the two different grade filtering methods (source 6 is excluded in these comparisons since it would otherwise dominate the results; we compute separate factors for source 6 of  $1.39 \pm 0.06$  and  $1.80 \pm 0.16$ ). We estimate that our fluxes have calibration uncertainties of  $\sim 30\%$ , but it is clear that we are detecting 2–8 keV sources *much* fainter than were detected with *ASCA* and *BeppoSAX*.

In addition to the sources described above, we will introduce two new sources below: source AG1 (found on S3 when *ASCA* grade filtering is used; see §2.4) and source I3 (found on ACIS CCD I3; see §3.2). To compute fluxes for source AG1, we have followed the method of the previous paragraph but have not made the grade correction (since we use *ASCA* grade filtering for this source). To compute fluxes for source I3, we again followed the method of the previous paragraph. However, ACIS I3 spectral responses are only available at present for a focal plane temperature of  $-90^{\circ}\text{C}$ . We have used these but recognize that this may introduce systematic error into our flux calculations for source I3. Therefore, we do not use the fluxes for source I3 in any of our subsequent analysis.

#### 2.4. Additional Safety Checks

The background level in the S3 CCD shows significant flaring during the observation due to ‘space weather’ (primarily soft electrons interacting with the CCD). We have repeated the analysis above after editing out the 8.0 ks when the background level was highest. We find the same 2–8 keV sources as those listed in Table 1 except that source 4 is not detected in the edited data set. Source 4 is detected in the 0.2–2 keV edited data, and we therefore believe that it is reliably detected in the hard band in the unedited data set (see Figure 2).

We have also performed source searches on images where we relax our grade screening so that we accept *ASCA* grades 0, 2, 3, 4 and 6. In these searches we detect most of the sources discussed in §2.2, but we fail to detect sources 2, 4 and 5 in the hard band. We thus infer a generally lower source detection efficiency with this grade screening. Our average background across S3 with this grade screening varies from  $\approx 0.07$ – $0.09$  count pixel $^{-1}$ , a factor of  $\approx 2$  higher than in §2.1 and §2.2. However, we do detect one new hard band source, which we will hereafter refer to as ‘source AG1’ (‘AG’ is for ‘*ASCA* grade’). We consider this source to be reliable since it is also detected in our independent soft band image, and we give its properties in Tables 1 and 2 (also see Figure 1). This source appears to have been missed by our source searching in §2.2 because several of its counts were rejected by our conservative grade filtering prescription. This highlights that it is difficult to choose a single optimal grade filtering criterion when dealing with sources with few counts; chance fluctuations in source grades can be important in this limit.

We have investigated if our choice of WAVDETECT wavelet scale sizes affects our results, and we find no evidence for this. We have repeated the searching of §2.2 using wavelet scale sizes of 1, 1.414, 2, 2.828, 4, 5.657, 8, 11.314 and 16 pixels (a ‘ $\sqrt{2}$  sequence’), and we find the same sources as in §2.2.

We are developing a matched filter code, based on the HRMA PSF, which we have used to check our WAVDETECT source detections. This preliminary matched filter code finds the same 9 hard-band sources on S3 that we have discussed in §2.1 and §2.2, and, like WAVDETECT, it finds soft-band counterparts for all sources other than source 5 (see §2.2).

We have also examined the spatial distribution of 2–8 keV sources on S3 to see if we can detect any spatial non-uniformity. We have used a two-dimensional ‘Kolmogorov-Smirnov test’ (see §14.7 of Press et al. 1992), and we have performed Monte-Carlo simulations to compute significance values for small numbers of sources. The 9 hard-band sources of §2.2 are found to be consistent with a uniform distribution. We have also performed the test including source AG1 (see above), and we found this sample of 10 sources to be consistent with a uniform distribution. However, we note that the two-dimensional ‘Kolmogorov-Smirnov test’ has limited statistical power for only 9–10 sources. In fact, we might have expected some spatial nonuniformity due to the fact that our sensitivity decreases away from the aim point; this may partially explain the absence of sources toward the lower-left part of Figure 1.

We have searched for spatial correspondences between our hard-band source positions and instrumental features, and we find none. In particular, we stress that sources 2, 3, 5 and 7 (the four blank-field sources of §3) are *not* linearly distributed along the dithered central node boundary (see §2.2 for a discussion of the node boundary). Source 7 is the closest of these four to the node boundary, and it is still  $9''$  from it (much larger than the PSF size at this position).

### 3. Optical Observations and Data Analysis

#### 3.1. Source Matching and Optical Photometry

We have compared the positions of our 2–8 keV sources with optical sources on the Palomar Optical Sky Survey (POSS) plates and an archival 600 s  $R$ -band image taken with the 2.5-m Isaac Newton Telescope (INT) on 19 October 1995 (see Figure 4 and §2.5 of Boyle et al. 1997). The INT image is sensitive down to  $R \approx 21.7$ . We take an optical source to be positionally coincident with a *Chandra* source when its centroid is within  $3''$  of the *Chandra* position in Table 1. Five of our nine sources from §2.2 are detected on the POSS plates. Two of these are AGN that have been previously identified by Boyle et al. (1997): the QSO CRSS J0030.6+2620 at  $z = 0.493$  (our source 6) and the Seyfert 2 CRSS J0030.7+2616 at  $z = 0.247$  (our source 8). The other four sources are not detected either on the POSS plates or in the deeper INT image, and these are henceforth referred to as ‘blank-field sources.’ The number of blank-field sources we have obtained appears reasonable when compared with an extrapolation to lower hard X-ray fluxes of the  $R$ -magnitude versus 2–10 keV flux relation shown in Figure 3 of Akiyama et al. (2000); we would expect optical counterparts with  $R \approx 18$ –23.5. It is also generally consistent with the results of deep soft X-ray surveys (compare with Figure 3 of Hasinger et al. 1999). We have used the APM catalog (McMahon & Irwin 1992) and the INT image to determine  $R$  magnitudes or  $R$ -magnitude limits for our sources; these are given in Table 2.

Source AG1 from §2.4 is not detected on the POSS plates, but it is coincident with a faint ( $R = 21.5$ ) object seen in the INT image.

Using the INT image, we find an  $R$ -band source density of 10.3 per square arcminute down to  $R = 21.7$ . Given this source density and our  $3''$  error circles, the probability that any given 2–8 keV source has a false optical counterpart is 0.08. However, we note that most of the counterparts have  $R$  magnitudes that are substantially brighter than the detection limit for the INT image, and their identifications are correspondingly more secure. The HET spectroscopy below combined with the rarity of AGN on the sky supports the correctness of our optical matching (see §4.1 of Schmidt et al. 1998 for details).

We have searched for NRAO VLA Sky Survey (NVSS; Condon et al. 1998) sources coincident with our X-ray sources and find none. This area of sky has not been covered by the VLA FIRST survey (Becker, White & Helfand 1995).

### 3.2. Hobby-Eberly Telescope Spectroscopy

We used the HET to obtain spectra for the three unidentified 2–8 keV sources from §2.2 with optical counterparts on the POSS plates. We also obtained a spectrum of the  $R = 19.1$  optical counterpart to a 2–8 keV source located on ACIS-I CCD I3 (see Table 1 for source details). We have not yet attempted to obtain an optical spectrum for source AG1.

The HET, located at McDonald Observatory, is the first optical/infrared 8-m class telescope to employ a fixed-altitude (Arecibo-type) design (Ramsey et al. 1998). All spectra were obtained in October 1999 with the Marcario Low Resolution Spectrograph (LRS; Hill et al. 1998; Hill et al. 2000; Schneider et al. 2000) mounted at the prime focus of the HET. A  $2.0''$  slit and  $300 \text{ line mm}^{-1}$  grism/GG385 blocking filter produced spectra from  $4400 \text{ \AA}$  to  $9000 \text{ \AA}$  at  $24 \text{ \AA}$  resolution. The exposure time per source ranged from 20–30 minutes. The image quality as delivered on the detector was typically  $2.5''$  (FWHM). Wavelength calibration was performed with a fourth-order polynomial fit to a set of Cd/Hg/Ne/Zn lines; the rms of the fit was  $0.8 \text{ \AA}$ . Observations of the spectrophotometric standards of Oke & Gunn (1983) were used to perform the relative flux calibration. Spectra of the four objects are displayed in Figure 5.

**Source 1:** Source 1 has  $\text{H}\alpha$  and  $[\text{O III}]$  emission at  $z = 0.269$ , with a derived absolute magnitude of  $M_B = -21.9$ . It has a large Balmer decrement with  $\text{H}\alpha/\text{H}\beta \gtrsim 10$ , and its optical continuum slope is red (for an AGN) with  $\alpha = -2.5 \pm 0.4$ .<sup>5</sup> The  $\text{H}\alpha$  line is resolved with a FWHM of  $1400 \text{ km s}^{-1}$ .

**Source 4:** Source 4 is definitely a  $z = 0.247$  galaxy ( $\text{H}\alpha$ ,  $[\text{O III}]$ , and  $[\text{O II}]$  emission, plus a strong Mg b absorption feature) with  $M_B = -21.3$ . Unfortunately, our spectrum did not permit a search for  $[\text{Ne V}]$  emission at  $3426 \text{ \AA}$  (compare with §4 of Schmidt et al. 1998). Its Balmer decrement is  $\text{H}\alpha/\text{H}\beta \gtrsim 3$ , and its optical continuum slope is  $\alpha = -1.8 \pm 0.4$ . The optical continuum emission is dominated by star light. The  $\text{H}\alpha$  line is unresolved with a FWHM of  $< 900 \text{ km s}^{-1}$ . With a 2–8 keV flux of  $4.1 \times 10^{-15} \text{ erg cm}^{-2} \text{ s}^{-1}$ , this is the faintest 2–8 keV source yet identified to our knowledge. Somewhat surprisingly, the redshift of this source is the same as that of CRSS J0030.7+2616 (our source 8), but we do not have any reason to suspect identification problems. A comparison of our HET spectrum (see Figure 5) and the spectrum for CRSS J0030.7+2616 given in Figure 1 of Boyle et al. (1995) shows that the equivalent width of  $\text{H}\alpha$  in CRSS J0030.7+2616 is  $\gtrsim 2$  times larger than that of source 4.

**Source 9:** Source 9 is difficult to interpret. The brightest optical source in the X-ray error circle is clearly extended on the INT image (see Figure 4). The optical counterpart is off the X-ray position by  $\approx 3''$ , which is by far the largest discrepancy of any of the optical identifications shown in Figure 4. The HET spectrum for this source shows one strong narrow line at  $7411 \text{ \AA}$  that is most likely  $\text{H}\alpha$  at  $z = 0.129$ . The line is unresolved with a FWHM of  $< 900 \text{ km s}^{-1}$ , and

---

<sup>5</sup> $F(\nu) \propto \nu^\alpha$ . Typical ‘blue’ quasars have  $-1.3 \lesssim \alpha \lesssim +0.1$ . Optical continuum slopes in this paper are for  $5500$ – $8800 \text{ \AA}$  in the observed frame.

the optical continuum is red with  $\alpha = -2.9 \pm 0.4$ . The residual ripple in the continuum below 7000 Å is an artifact due to incomplete cancellation of fringing from a pellicle by the flat field. The relatively large difference between the optical and X-ray positions suggests that this may not be the correct identification. Another possibility is that this galaxy is a member of a small group and that the X-ray emission arises from the general environment and not an individual galaxy. However, the hard X-ray spectral shape would be difficult to understand in this case.

**Source I3:** Source I3 is a strong-lined quasar at  $z = 1.665$  with  $M_B = -24.7$ . The lines shown in Figure 5 have FWHM of  $\approx 5000 \text{ km s}^{-1}$ , and the optical continuum slope of  $\alpha = -1.2 \pm 0.4$  is consistent with that of ‘normal’ blue quasars.

Using our HET spectrum, we estimate  $(V - R) \approx +0.3$  for source I3. For the other sources we estimate  $(V - R) \approx +0.5$ .

### 3.3. The Blank-Field Sources

We have compared the properties of the blank-field sources to those of the other sources to gain clues to their nature. Examination of Figure 6 shows that the blank-field sources are not the faintest 2–8 keV sources in our sample; we have obtained successful HET identifications for sources with comparable or smaller 2–8 keV fluxes. This is comforting in that it suggests that our blank-field sources are indeed reliable X-ray detections. Figures 6a and 6b also show that the blank-field sources have larger X-ray to  $V$ -band flux ratios than the other sources, as expected. However, these X-ray to  $V$ -band flux ratios are still consistent with those expected for AGN (compare with Figure 1 of Maccacaro et al. 1988). Figure 6c suggests that the blank-field sources may be somewhat harder than the other sources, but we do not consider this result to be statistically significant at present.

If the blank-field X-ray sources are in normal  $L^*$  galaxies (Kirshner et al. 1983; Efstathiou, Ellis & Peterson 1988), they must be at moderately high redshifts to explain their nondetections in the INT image (corresponding to  $R > 21.7$ ). To avoid detection in the INT image, an  $L^*$  Scd galaxy must have  $z \gtrsim 0.75$ , and an  $L^*$  elliptical,  $z \gtrsim 0.55$ . Typical  $L^*$  galaxies would thus need to be at higher redshifts than that of the cluster CRSS J0030.5+2618. The moderately high redshifts required for host galaxies also serve to rule out single extragalactic X-ray binaries and other low-luminosity X-ray sources associated with galaxies from creating the observed X-ray emission (unless the host galaxies have extremely low optical luminosities; we would have detected a host galaxy that is sub- $L^*$  by two magnitudes to  $z = 0.2$ ). Large hard X-ray luminosities of  $L_{2-8} \gtrsim 5 \times 10^{41} \text{ erg s}^{-1}$  are required for  $z \gtrsim 0.2$ . Such hard X-ray luminosities are commonly seen among local AGN. They might also be generated by the most extreme ‘pure’ starburst galaxies, although even the most X-ray luminous starbursts known at present have hard X-ray luminosities  $\lesssim 3 \times 10^{41} \text{ erg s}^{-1}$  (e.g., Moran, Lehnert & Helfand 2000). In addition, the X-ray spectra of the blank-field sources are significantly harder than those seen for ‘pure’ starbursts at low redshift.

If the blank-field X-ray sources are ‘bona-fide’ quasars, with  $M_B < -22.3$  for our adopted cosmology, they would need to have  $z > 1.75$  to avoid detection on the INT image. Quasars with  $z < 3$  and  $M_B < -23.2$  would have been seen in the INT image, and a quasar as luminous as 3C273 would have been detected at redshifts greater than 4.

#### 4. Discussion and Conclusions

Our results, obtained from a small but well-defined sample of 2–8 keV sources, extend previous X-ray background studies in several ways. First, we have detected and securely identified hard X-ray sources about an order of magnitude fainter than has previously been possible. At our 2–8 keV flux limit of  $\approx (4\text{--}8) \times 10^{-15}$  erg cm $^{-2}$  s $^{-1}$  (spatially dependent; see §2.2), we find ten sources (including AG1) in our 63.5 arcmin $^2$  search area, corresponding to a 2–8 keV source density of  $570 \pm 180$  deg $^{-2}$ . Even allowing for the possibility of one spurious source detection, this source density is still  $\approx 10$  times larger than previous number counts in this energy band (e.g., Ogasaka et al. 1998; Giommi et al. 1998), and down to  $\approx 2 \times 10^{-14}$  erg cm $^{-2}$  s $^{-1}$  our number counts appear consistent with the *ASCA* fluctuation analyses of Gendreau et al. (1998). However, our source counts may be somewhat enhanced due to the presence of the cluster CRSS J0030.5+2618 (see below). The fact that we detect sources down to  $\approx 4 \times 10^{-15}$  erg cm $^{-2}$  s $^{-1}$  suggests that the number counts versus flux relation departs from the Euclidean form (the X-ray background would be resolved at  $\approx 10^{-14}$  erg cm $^{-2}$  s $^{-1}$  without a break in the log  $N$ –log  $S$  slope), although further data are clearly needed to quantify the break parameters.

Four of our five S3 sources with optical spectroscopy have  $z < 0.3$ , which clearly exclude them from being associated with the cluster CRSS J0030.5+2618 at  $z = 0.516$ . The fifth, the QSO CRSS J0030.6+2620, differs in redshift from the cluster by  $\Delta z = 0.023$  corresponding to a line-of-sight separation of  $\approx 100$  Mpc. While this QSO is certainly not a bound member of the cluster, it could be associated with the large-scale cosmic structure producing the cluster. As discussed in §3.3, if any of our blank-field sources (or AG1) lie in the cluster, they must be sub- $L^*$  galaxies producing large hard X-ray luminosities of  $L_{2\text{--}8} \gtrsim 4 \times 10^{42}$  erg s $^{-1}$ . Even in the most conservative (and unlikely) case, where we allow all objects with unknown  $z$  to lie in the cluster, our cluster-corrected source density is still a factor of  $\approx 4.5$  times higher than previously attained by *ASCA* and *BeppoSAX*. The same statement obtains for possible gravitational lensing effects by the cluster.

We detect nine of our ten 2–8 keV sources in the 0.2–2 keV band. While our statistics are admittedly limited, this result is consistent with the finding by Giommi, Fiore & Perri (1998) that most hard X-ray sources have soft X-ray counterparts, and it extends this result downward in flux by about an order of magnitude (see §1 for discussion). Down to our flux limit, we can show with  $> 90\%$  confidence that hard-band only sources comprise  $< 40\%$  of the total hard-band source population. Deeper *Chandra* observations are needed to determine if a large population of hard-band only sources emerges at still fainter flux levels.

We thank C.S. Crawford and A.C. Fabian for providing the archival INT image, G.M. Hill and M. Shetrone for help with the HET data acquisition, P.S. Broos, A.C. Fabian, E.D. Feigelson and G. Hasinger for helpful discussions, and D.H. Saxe for valuable computer support. We thank all the members of the *Chandra* team for their enormous efforts. We gratefully acknowledge the financial support of NASA grant NAS 8-38252 (GPG, PI), NASA LTSA grant NAG5-8107 (WNB), NASA GSRP grant NGT5-50247 (AEH), and NSF grant AST99-00703 (DPS). The HET is a joint project of the University of Texas at Austin, the Pennsylvania State University, Stanford University, Ludwig-Maximilians-Universität München, and Georg-August-Universität Göttingen. The HET is named in honor of its principal benefactors, William P. Hobby and Robert E. Eberly. The Marcario LRS is a joint project of the University of Texas at Austin, the Instituto de Astronomia de la Universidad Nacional Autonoma de Mexico, Ludwig-Maximilians-Universität München, Georg-August-Universität Göttingen, Stanford University, and the Pennsylvania State University. This research is partially based upon data from the Isaac Newton Group archive.

Table 1. Basic X-ray Properties of the 2–8 keV Sources.

Source Name	X-ray $\alpha_{2000}$	X-ray $\delta_{2000}$	Aim point distance (')	0.2–2 keV counts	2–8 keV counts	Hard/Soft ratio	0.2–2 keV significance	2–8 keV significance
1	00 <sup>h</sup> 30 <sup>m</sup> 26.0 <sup>s</sup>	+26° 16' 48.9"	2.0	128.4 ± 11.5	9.4 ± 3.2	0.073 ± 0.026	41.8	4.4
2	00 <sup>h</sup> 30 <sup>m</sup> 27.8 <sup>s</sup>	+26° 15' 14.9"	3.1	36.4 ± 6.6	9.2 ± 3.6	0.25 ± 0.11	6.8	3.0
3	00 <sup>h</sup> 30 <sup>m</sup> 30.8 <sup>s</sup>	+26° 16' 00.0"	2.2	30.8 ± 5.7	12.0 ± 3.6	0.39 ± 0.14	11.3	5.2
4	00 <sup>h</sup> 30 <sup>m</sup> 33.3 <sup>s</sup>	+26° 14' 50.9"	3.3	34.9 ± 6.1	6.2 ± 2.6	0.18 ± 0.08	13.1	2.8
5	00 <sup>h</sup> 30 <sup>m</sup> 34.7 <sup>s</sup>	+26° 16' 29.8"	1.8	< 7.5	8.1 ± 3.0	> 0.68	...	3.6
6	00 <sup>h</sup> 30 <sup>m</sup> 39.5 <sup>s</sup>	+26° 20' 54.9"	3.1	1830.5 ± 43.0	413.1 ± 20.4	0.23 ± 0.01	355.3	122.4
7	00 <sup>h</sup> 30 <sup>m</sup> 42.6 <sup>s</sup>	+26° 17' 46.1"	2.3	21.9 ± 4.9	11.9 ± 3.6	0.54 ± 0.23	8.1	5.1
8	00 <sup>h</sup> 30 <sup>m</sup> 47.8 <sup>s</sup>	+26° 16' 47.0"	3.7	141.9 ± 12.3	27.8 ± 5.7	0.20 ± 0.04	34.3	8.0
9	00 <sup>h</sup> 30 <sup>m</sup> 51.3 <sup>s</sup>	+26° 17' 11.9"	4.3	99.4 ± 10.4	42.1 ± 6.9	0.42 ± 0.09	23.5	11.8
AG1	00 <sup>h</sup> 30 <sup>m</sup> 41.6 <sup>s</sup>	+26° 17' 40.8"	2.1	65.9 ± 8.3	13.1 ± 4.0	0.20 ± 0.07	22.4	4.5
I3	00 <sup>h</sup> 31 <sup>m</sup> 08.4 <sup>s</sup>	+26° 20' 56.3"	8.5	136.4 ± 12.4	36.5 ± 6.9	0.27 ± 0.06	26.4	8.4

Sources 1–9 are located on the S3 CCD and source I3 is located on the I3 CCD; properties for these sources have been found using filtering on ACIS grades 0, 2, 8, 16 and 64. Source AG1 is only found when *ASCA* grade filtering is used (see §2.4); properties for this source have been found using filtering on *ASCA* grades 0, 2, 3, 4 and 6. Note that we have only listed the sources that are detected in the 2–8 keV band.

Table 2. X-ray Fluxes/Luminosities and Optical Properties of the 2–8 keV Sources.

Source Name	0.2–2 keV flux (erg cm <sup>-2</sup> s <sup>-1</sup> )	2–8 keV flux (erg cm <sup>-2</sup> s <sup>-1</sup> )	2–8 keV $L_X$ (erg s <sup>-1</sup> )	$R$	$z$	Notes <sup>a</sup>
1	$1.0 \times 10^{-14}$	$6.0 \times 10^{-15}$	$1.1 \times 10^{42}$	18.4	0.269	HET
2	$2.9 \times 10^{-15}$	$5.9 \times 10^{-15}$	...	> 21.7	...	BF
3	$2.5 \times 10^{-15}$	$7.7 \times 10^{-15}$	...	> 21.7	...	BF
4	$2.9 \times 10^{-15}$	$4.1 \times 10^{-15}$	$6.1 \times 10^{41}$	18.7	0.247	HET
5	< $5.9 \times 10^{-16}$	$5.2 \times 10^{-15}$	...	> 21.7	...	BF
6	$1.6 \times 10^{-13}$	$3.3 \times 10^{-13}$	$2.1 \times 10^{44}$	16.9	0.493	CRSS J0030.6+2620 (QSO)
7	$1.7 \times 10^{-15}$	$7.7 \times 10^{-15}$	...	> 21.7	...	BF
8	$1.1 \times 10^{-14}$	$1.8 \times 10^{-14}$	$2.7 \times 10^{42}$	18.5	0.247	CRSS J0030.7+2616 (Seyfert 2)
9	$8.0 \times 10^{-15}$	$2.9 \times 10^{-14}$	$1.1 \times 10^{42}$ <sup>b</sup>	19.1	0.129 <sup>b</sup>	HET
AG1	$4.2 \times 10^{-15}$	$5.5 \times 10^{-15}$	...	21.5	...	<i>ASCA</i> grade source
I3	$1.9 \times 10^{-14}$	$2.0 \times 10^{-14}$	$1.9 \times 10^{44}$	19.1	1.665	HET

<sup>a</sup>Sources noted as ‘HET’ are those for which we present HET spectra, and sources noted as ‘BF’ (for ‘Blank Field’) are those without optical counterparts.

<sup>b</sup>We consider this redshift and luminosity to be only tentative (see §3.2 for details).

## REFERENCES

Akiyama, M., et al. 2000, ApJ, in press (astro-ph/0001289)

Baganoff, F. 1999, ACIS On-Orbit Background Rates and Spectra from OAC Phase 1. Massachusetts Institute of Technology, Cambridge

Becker, R.H., White, R.L. & Helfand, D.J. 1995, ApJ, 450, 559

Bevington, P.R. & Robinson, D.K. 1992, Data Reduction and Error Analysis for the Physical Sciences: Second Edition. McGraw Hill, New York

Boyle, B.J., McMahon, R.G., Wilkes, B.J. & Elvis, M. 1995, MNRAS, 276, 315

Boyle, B.J., Wilkes, B.J. & Elvis, M. 1997, MNRAS, 285, 511

Broos, P. et al. 1999, User's Guide for the TARA Package: Document Revision 5.3. Penn State University, University Park (available at <http://www.astro.psu.edu/xray/docs/>)

Condon, J.J., Cotton, W.D., Greisen, E.W., Yin, Q.F., Perley, R.A., Taylor, G.B. & Broderick, J.J. 1998, AJ, 115, 1693

Dobrzański, A., Ebeling, H., Glotfelty, K., Freeman, P., Damiani, F., Elvis, M. & Calderwood, T. 1999, *Chandra* Detect 1.0 User Guide. *Chandra* X-ray Center, Cambridge

Efstathiou, G., Ellis, R.S. & Peterson, B.A. 1988, MNRAS, 232, 431

Fiore, F., La Franca, F., Giommi, P., Elvis, M., Matt, G., Comastri, A., Molendi, S. & Gioia I. 1999, MNRAS, 306, L55

Freeman, P.E., Kashyap, V., Rosner, R. & Lamb, D.Q. 2000, ApJ, submitted

Garmire, G.P. & Nousek, J.A. 1999a, Science Instrument Operations Handbook for the Advanced CCD Imaging Spectrometer. Penn State University, University Park (available at <http://www.astro.psu.edu/xray/docs/sop/sop.html>)

Garmire, G.P. & Nousek, J.A. 1999b, Preliminary Status Report: ACIS Front-Illuminated CCD Detector Anomaly. Penn State University, University Park (available at <http://www.astro.psu.edu/xray/axaf/index.html>)

Gehrels, N. 1986, ApJ, 303, 336

Gendreau, K.C., Barcons, X. & Fabian, A.C. 1998, MNRAS, 297, 41

Giommi, P., Fiore, F. & Perri, M. 1999, in Proceedings of the 3rd Integral Workshop, (ESA Press, Noordwijk), in press (astro-ph/9812305)

Hasinger, G., Burg, R., Giacconi, R., Hartner, G., Schmidt, M., Trümper, J. & Zamorani, G. 1993, *A&A*, 275, 1 (erratum *A&A*, 291, 348)

Hasinger, G., Burg, R., Giacconi, R., Schmidt, M., Trümper, J. & Zamorani, G. 1998, *A&A*, 329, 482

Hasinger, G., Lehmann, I., Giacconi, R., Schmidt, M., Trümper, J. & Zamorani, G. 1999, in *Highlights in X-ray Astronomy*, (MPE Press, Garching), in press (astro-ph/9901103)

Hill, G.J., Nicklas, H.E., MacQueen, P.J., Tejada, C., Cobos Duenas, F.J. & Mitsch, W. 1998, *Proc. SPIE*, 3355, 375

Hill, G.J., et al. 2000, *PASP*, in press

Kirshner, R.P., Oemler, A., Schechter, P.L. & Shectman, S.A. 1983, *AJ*, 88, 1285

Lyons, L. 1991, *Data Analysis for Physical Science Students*. Cambridge University Press, Cambridge

Maccacaro, T., Gioia, I.M., Wolter, A., Zamorani, G. & Stocke, J.T. 1988, *ApJ*, 326, 680

McMahon, R.G. & Irwin, M.J. 1992, in *Digitised Optical Sky Surveys*, ed. MacGillivray, H. T. & Thomson, E. B. (Kluwer, Dordrecht), p. 417

Moran, E.C., Lehnert, M.D. & Helfand, D.J. 2000, *ApJ*, in press (astro-ph/9907036)

Ogasaka, Y., et al. 1998, *Astr. Nach.*, 319, 43

Oke, J.B. & Gunn, J.E. 1983, *ApJ*, 266, 713

Press, W.H., Teukolsky, S.A., Vetterling, W.T. & Flannery, B.P. 1992, *Numerical Recipes in C: Second Edition*. Cambridge University Press, Cambridge

Ramsey, L.W., et al. 1998, *Proc. SPIE*, 3352, 34

Schmidt, M., Hasinger, G., Gunn, J., Schneider, D., Burg, R., Giacconi, R., Lehmann, I., MacKenty, J., Trümper, J. & Zamorani, G. 1998, *A&A*, 329, 495

Schneider, D.P., et al. 2000, *PASP*, in press (astro-ph/9910306)

Stark, A.A., Gammie, C.F., Wilson, R.W., Bally, J., Linke, R.A., Heiles, C. & Hurwitz, M. 1992, *ApJS*, 79, 77

Stocke, J.T., Morris, S.L., Gioia, I.M., Maccacaro, T., Schild, R., Wolter, A., Fleming, T.A. & Henry, J.P. 1991, *ApJS*, 76, 813

Ueda, Y., et al. 1998, *Nature*, 391, 866

Weisskopf, M.C., O'Dell, S.L. & van Speybroeck, L. 1996, *SPIE*, 2805, 2



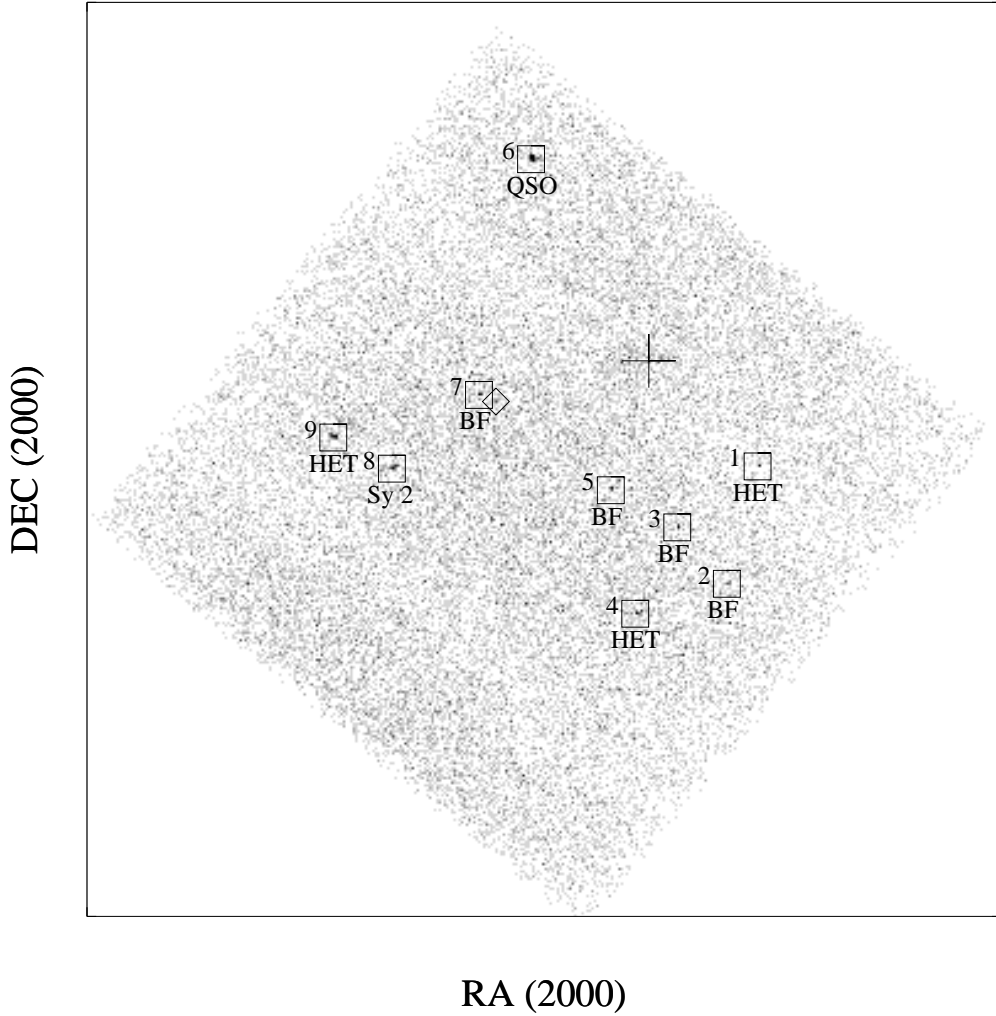


Fig. 1.— Image of the ACIS S3 CCD from 2–8 keV with the WAVDETECT sources marked and numbered. The box sizes are arbitrary ( $\approx 20''$  on a side); the positional accuracy is much better than the box size. The cross shows the position of the aim point and the cluster CRSS J0030.5+2618 ( $z = 0.516$ ), and the diamond near source 7 shows the position of source AG1 (see §2.4). The QSO CRSS J0030.6+2620 ( $z = 0.493$ ) and the Seyfert 2 CRSS J0030.7+2616 ( $z = 0.247$ ) are labeled as ‘QSO’ and ‘Sy 2’, respectively. Sources for which we present HET spectra are labeled ‘HET’ and sources without optical counterparts are labeled ‘BF’ (for ‘Blank Field’). North is at the top, and East is to the left. For scale, the CCD is 8.3' on a side.

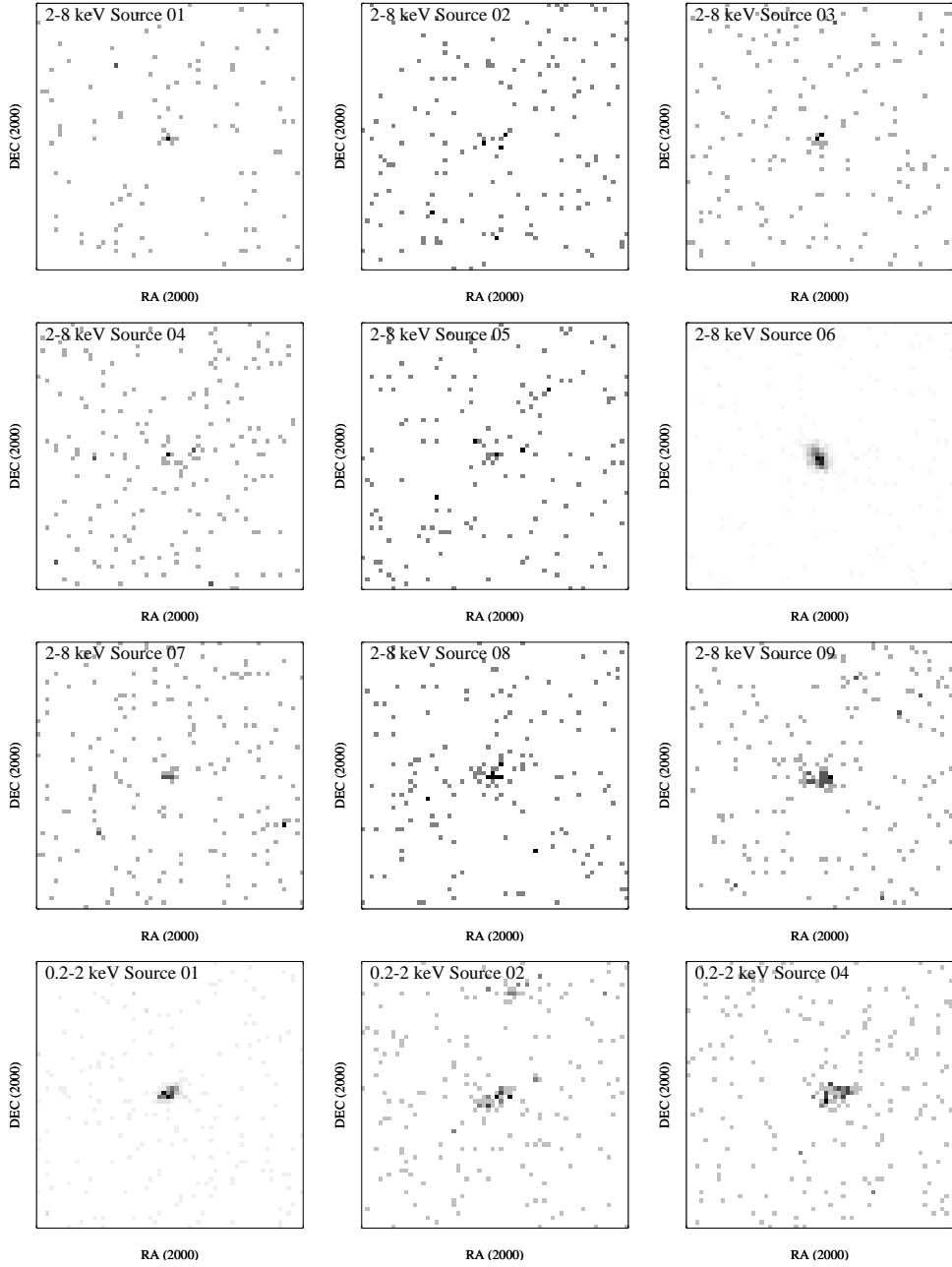


Fig. 2.— ACIS images of the 2–8 keV sources from the S3 CCD. Each image is centered on the corresponding position from Table 1, and each is  $30''$  on a side. Each pixel is  $0.5''$  on a side. To further demonstrate the reality of sources 1, 2 and 4, we also show their independent 0.2–2 keV images. The grayscale levels are linear and vary from image to image, but white corresponds to zero in all images. Most of the non-white pixels away from the sources themselves have one count.

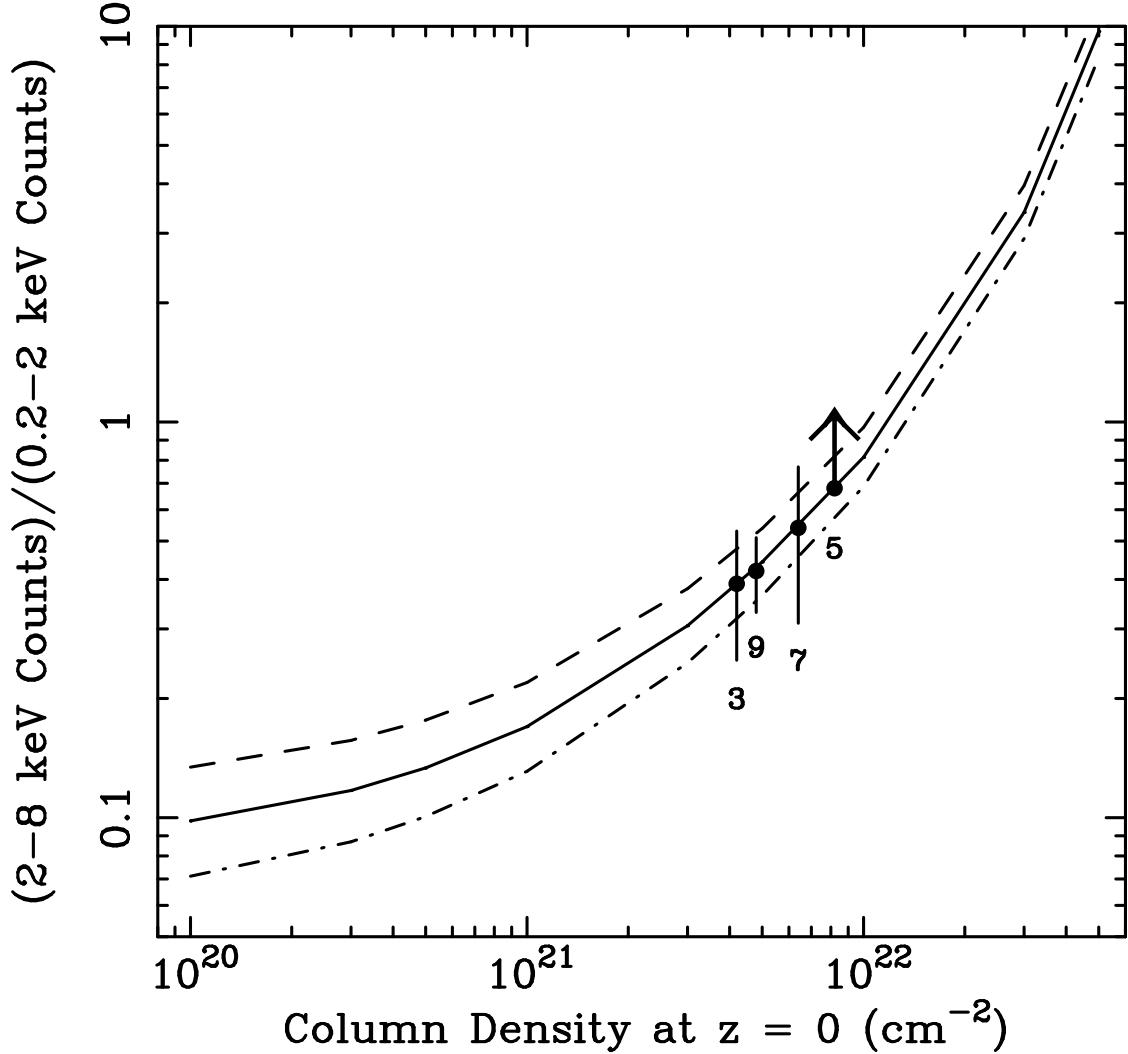


Fig. 3.— Plot of the hard-band to soft-band ratio versus column density at  $z = 0$  for power-law models with photon indices of  $\Gamma = 1.7$  (dashed curve),  $\Gamma = 1.9$  (solid curve) and  $\Gamma = 2.1$  (dot-dashed curve). The data points show the band ratios for sources 3, 5, 7 and 9 (the hardest sources we find). These sources have been arbitrarily placed on the  $\Gamma = 1.9$  curve; better X-ray spectra would be needed to determine their underlying photon indices. Provided these sources have intrinsic X-ray continua that are similar to those of Seyferts and QSOs, they appear to have column densities larger than a few times  $10^{21} \text{ cm}^{-2}$ . Source 5 is likely to have a column density  $\gtrsim 10^{22} \text{ cm}^{-2}$ . Note that the probable absorption for these sources is presumably intrinsic, and thus correcting for the effects of redshift will only increase the inferred column densities. The curves have been calculated assuming only ACIS grade 0, 2, 8, 16 and 64 events are used.

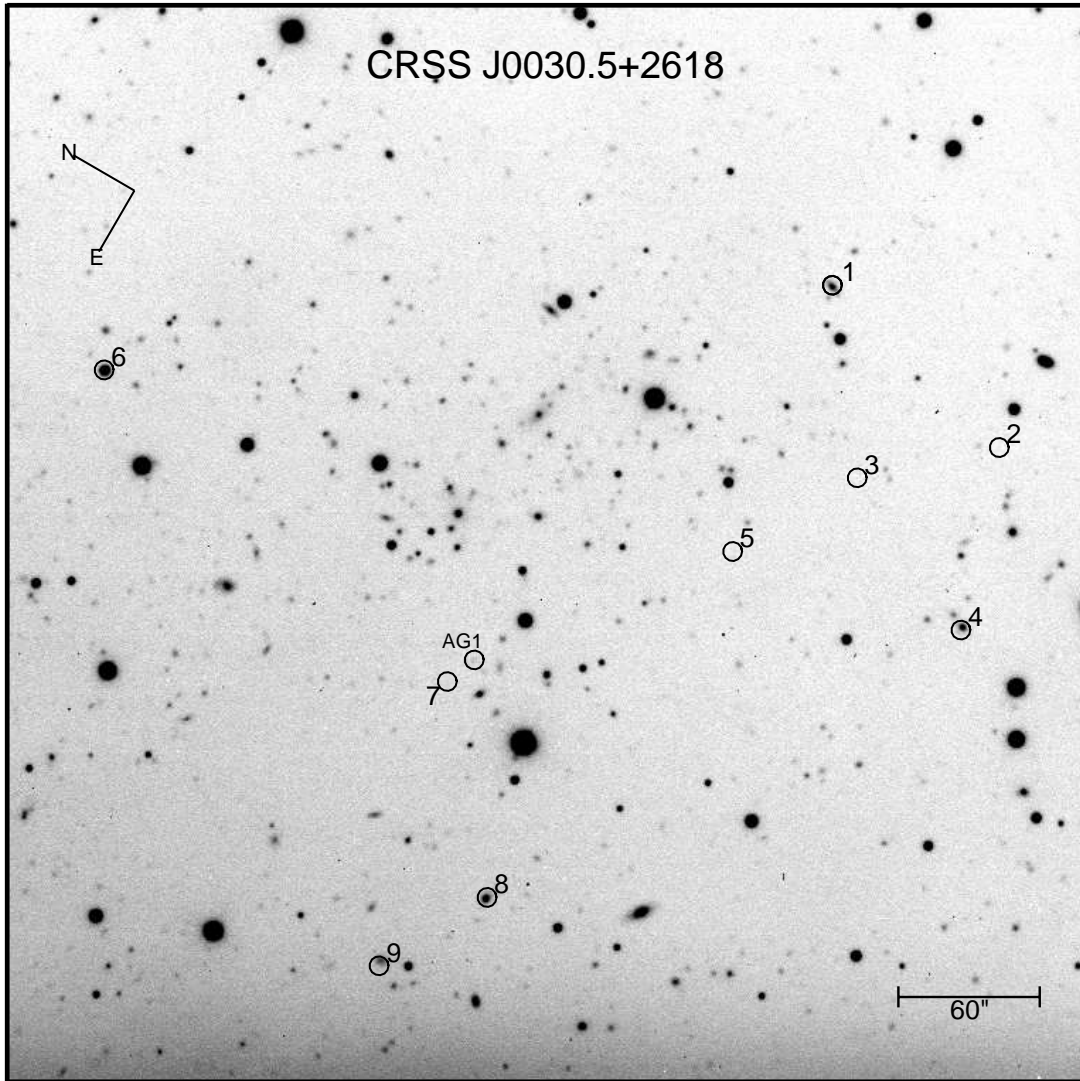


Fig. 4.— INT image of the field of the cluster CRSS J0030.5+2618. The field is 7.5' on a side. We have marked our *Chandra* sources with circles of 4'' radius (note that this is somewhat larger than our positional uncertainty). The cluster is located about 1' North of source 5.

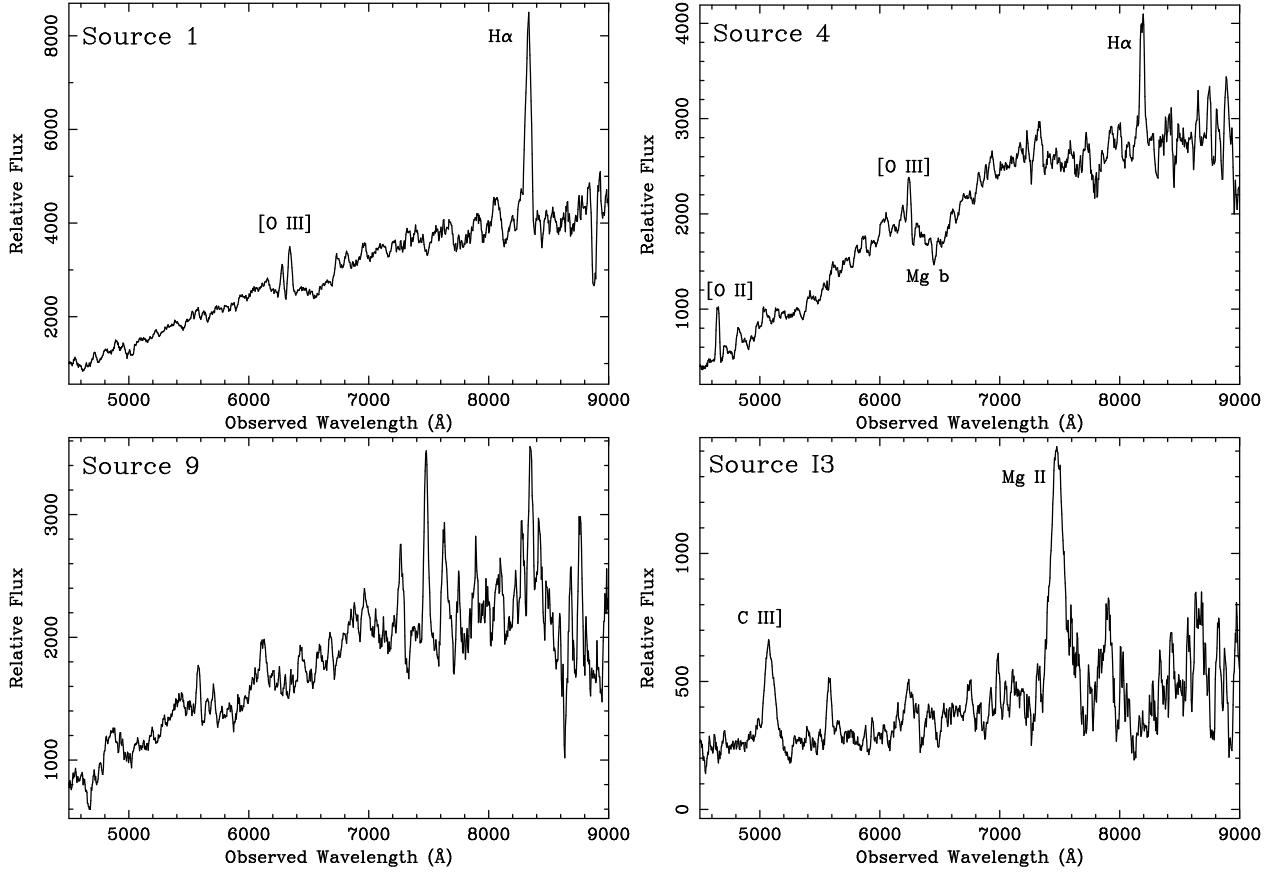


Fig. 5.— HET LRS spectra for the *Chandra* sources 1, 4, 9 and I3. The spectral resolution is 24 Å.

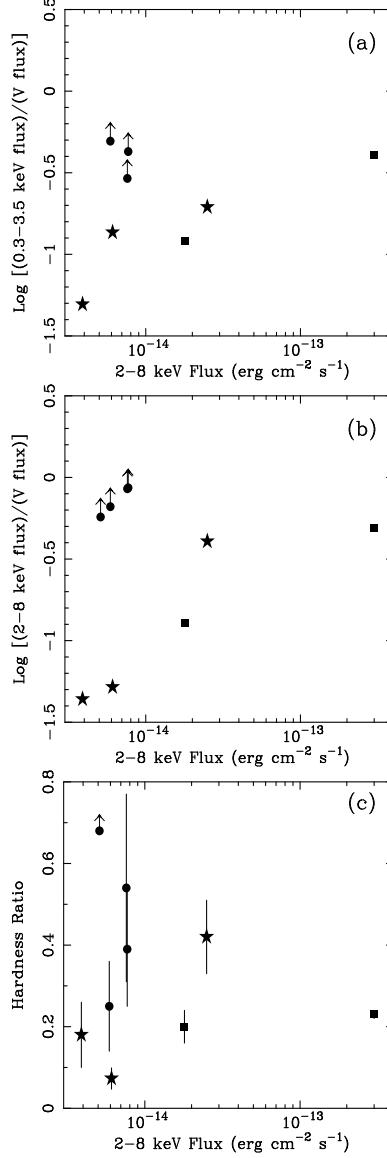


Fig. 6.— X-ray to  $V$ -band flux ratios and X-ray band ratios for our sources. Stars indicate sources with HET spectra, squares indicate CRSS sources, and solid dots indicate blank-field sources. Source 5 is not plotted in panel (a) because it does not have a soft-band detection, and two of the solid dots overlap in panel (b). The fluxes used in panels (a) and (b) are corrected for absorption by the Galaxy. Panel (a) is plotted for 0.3–3.5 keV for comparison with the X-ray to  $V$ -band flux ratios given by Stocke et al. (1991) and Schmidt et al. (1998). Our X-ray to  $V$ -band flux ratios are on average somewhat smaller than those found by these authors, probably a selection effect due to our sensitive X-ray data and our relatively shallow optical data.